JACS
JOURNAL OF THE AMERICAN CHEMICAL SOCIETY
pubs.acs.org/JACS
Communication

Hybrid Layered Double Perovskite Halides of Transition Metals

Pratap Vishnoi, Julia L. Zuo, Xiaotong Li, Devesh Chandra Binwal, Kira E. Wyckoff, Lingling Mao, Linus Kautzsch, Guang Wu, Stephen D. Wilson, Mercouri G. Kanatzidis, Ram Seshadri,* and Anthony K. Cheetham*

Cite This: J. Am. Chem. Soc. 2022, 144, 6661−6666
Read Online

ABSTRACT: Hybrid layered double perovskite (HLDP) halides comprise hexacoordinated 1+ and 3+ metals in the octahedral sites within a perovskite layer and organic amine cations between the layers. Progress on such materials has hitherto been limited to compounds containing main group 3+ ions isoelectronic with Pb^{II} (such as Sb^{III} and Bi^{III}). Here, we report eight HLDP halides from the $A_2M^IM^{III}X_8$ family, where A = *para*-phenylenediammonium (PPDA), 1,4-butanediammonium (1,4-BDA), or 1,3-propanediammonium (1,3-PDA); M^I = Cu or Ag; M^{III} = Ru or Mo; X = Cl or Br. The optical band gaps, which lie in the range 1.55 to 2.05 eV, are tunable according to the layer composition, but are largely independent of the spacer. Magnetic measurements carried out for $(PPDA)_2Ag^IRu^{III}Cl_8$ and $(PPDA)_2Ag^IMo^{III}Cl_8$ show no obvious evidence of a magnetic ordering transition. While the t_{2g}^3 Mo^{III} compound displays Curie−Weiss behavior for a spin-only d^3 ion, the t_{2g}^5 Ru^{III} compound displays marked deviations from the Kotani theory.

Hybrid layered halide perovskites possess useful optoelectronic properties with some appealing characteristics when compared with their 3D analogues. They show greater ambient stability, rich chemical and structural diversity, ease of device fabrication, and exquisite tunability of properties.[1,2] A recent development in the area is the discovery of hybrid layered double perovskite (HLDP) halides, formed by an ordered arrangement of monovalent and trivalent metals in the 2D perovskite layers with large organic amine cations separating and charge-balancing the layers.[3] When diammonium cations separate the layers, Dion−Jacobson (DJ) type structures with eclipsed stacking of the layers are formed in one of the two ways, i.e., [0, 0] or [1/2, 0] (Figure 1).

Owing to the enormous interest in their optoelectronic properties, 3+ metals that are isoelectronic with Pb^{II}, such as Sb^{III} and Bi^{III}, have been utilized to form a number of HLDP halides. Typical examples include $(1,4\text{-BDA})_2AgBiBr_8$,[4] $(AE2\text{-}T)_2AgBiI_8$,[5] $(AMP)_4[AgBiI_8]_2{\cdot}H_2O$,[6] $(CHDA)_2CuBiI_8{\cdot}0.5H_2O$,[7] $(CHDA)_2AgBiI_8{\cdot}H_2O$,[7] $(MPDA)_2CuBiI_8$,[8] and $(3AMPY)_2AgBiI_8{\cdot}H_2O$ (Table S1).[9−11]

There has separately been considerable progress in the development of layered single perovskite halides of 2+ transition metals (TMs).[12−16] In addition, there is a report of mixed-valence Au^+/Au^{3+} based perovskite iodides containing $[Au^IAu^{III}I_6]^{2-}$ layers of linear $[Au^II_2]^-$ and square planar $[Au^{III}I_4]^-$ ions.[17] However, the family of typical HLDP halides has not yet been extended to heterometallic and magnetic systems with 1+ and 3+ TMs. This could be attributable to synthetic challenges arising from the existence of other oxidation states in addition to the required 1+ and 3+ states. The unfavorable tolerance factors of many of the hypothetical 3D halide perovskites may also impact the ability to synthesize several of the corresponding layered structures.[18]

In terms of magnetic properties, there is great current interest in geometrically frustrated oxides and halides of spin 1/2 metals. Layered α-$RuCl_3$, with its t_{2g}^5 Ru^{III} configuration and strong spin−orbit coupling (SOC), is an important example of a Kitaev quantum spin liquid.[19] The influence of SOC on the magnetism of Ru^{III} and Ru^{IV} perovskites has also recently been studied.[20,21] These developments have encouraged us to successfully attempt the incorporation of Ru^{III} ($4d^5$) and Mo^{III} ($4d^3$) into eight prototype HLDP halides with the $A_2M^IM^{III}X_8$ composition (Table 1), where A = *para*-phenylenediammonium, 1,4-butanediammonium and 1,3-propanediammonium (hereafter abbreviated as PPDA, 1,4-BDA and 1,3-PDA, respectively); M^I = Cu and Ag; M^{III} = Ru and Mo; X = Cl and Br. Their structures, optical properties, and magnetism are discussed below.

The synthesis of the compounds **1**−**8** was accomplished by controlling the oxidation state of the trivalent transition metals by using hypophosphorus acid as a reducing agent.[20] In the absence of H_3PO_2, oxidation of Ru^{III} and Mo^{III} to Ru^{IV} and Mo^{IV} takes place, which prevents the synthesis of the desired products. The compounds are monolayer DJ perovskites comprising fully ordered metal ions and halides in the $[M^IM^{III}X_8]^{4-}$ layers, which are separated by doubly protonated A cations in the stacking direction. The $[M^IX_6]$ polyhedra are distorted with axial compression, while the $[M^{III}X_6]$ polyhedra are nearly regular octahedra. We attribute the smaller distortion around 3+ metal ions to the stronger M^{III}−X bonds, as well as the large crystal

Received: December 3, 2021
Published: April 4, 2022

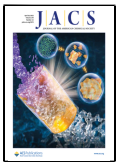

https://doi.org/10.1021/jacs.1c12760
J. Am. Chem. Soc. 2022, 144, 6661−6666

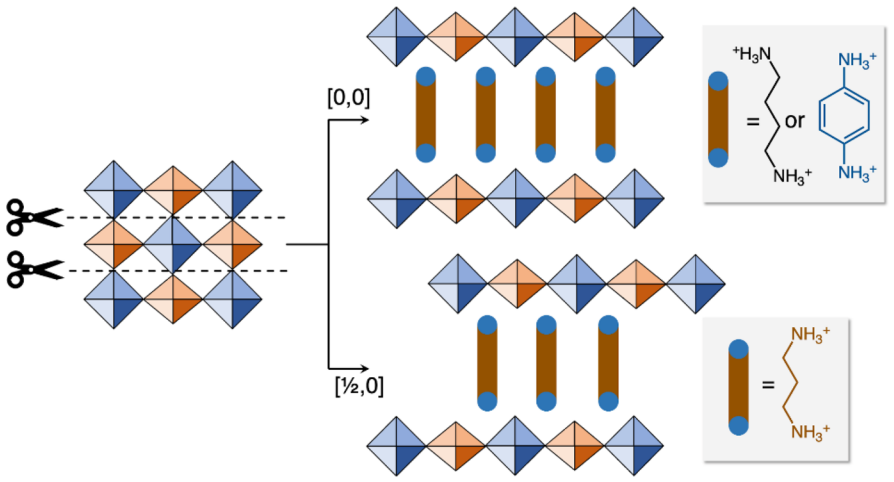

Figure 1. [0, 0] and [1/2, 0] stacking patterns that can be found in (100)—oriented monolayer DJ type HLDP halides. In the former, the successive layers show almost no in-plane displacement, though the layers are eclipsed. They are eclipsed in the latter, too, but consecutive layers show approximately half a unit cell displacement along one of the in-plane axes. The diammonium cations used in this study are also shown.

Table 1. Chemical Composition, Structural Parameters and Optical Band Gaps of the HLDP Halides Described in this Study

Compound	Stacking pattern	Interlayer spacing (Å)	Symmetry	Glazer tilt system	Band gap (eV)
$(PPDA)_2AgRuCl_8$ (**1**)	[0, 0]	10.14	Triclinic, $P\bar{1}$	a^-b^-c	1.80
$(PPDA)_2CuRuCl_8$ (**2**)	[0, 0]	9.97	Triclinic, $P\bar{1}$	a^-b^-c	1.55
$(PPDA)_2AgRuBr_8$ (**3**)	[0, 0]	10.26	Triclinic, $P\bar{1}$	a^-b^-c	1.67
$(PPDA)_2AgMoCl_8$ (**4**)	[0, 0]	10.19	Triclinic, $P\bar{1}$	a^-b^-c	2.05
$(1,4\text{-}BDA)_2AgRuCl_8$ (**5**)	[0, 0]	10.40	Monoclinic, $C2/m$	$a^0b^-c^0$	1.89
$(1,4\text{-}BDA)_2AgRuBr_8$ (**6**)	[0, 0]	9.35	Triclinic, $P\bar{1}$	a^-b^-c	1.60
$(1,3\text{-}PDA)_2AgRuCl_8$ (**7**) 300 K	[1/2, 0]	9.11	Monoclinic, $C2/m$	$a^0b^-c^0$	1.86
$(1,3\text{-}PDA)_2AgRuCl_8$ (**7**) 220 K	[1/2, 0]	8.64	Monoclinic, $C2/m$	$a^-a^-c^0/a^-a^-c^0$	–
$(1,3\text{-}PDA)_2AgRuBr_8$ (**8**)	[1/2, 0]	8.82	Monoclinic, $C2/m$	$a^-a^-c^0/a^-a^-c^0$	1.70

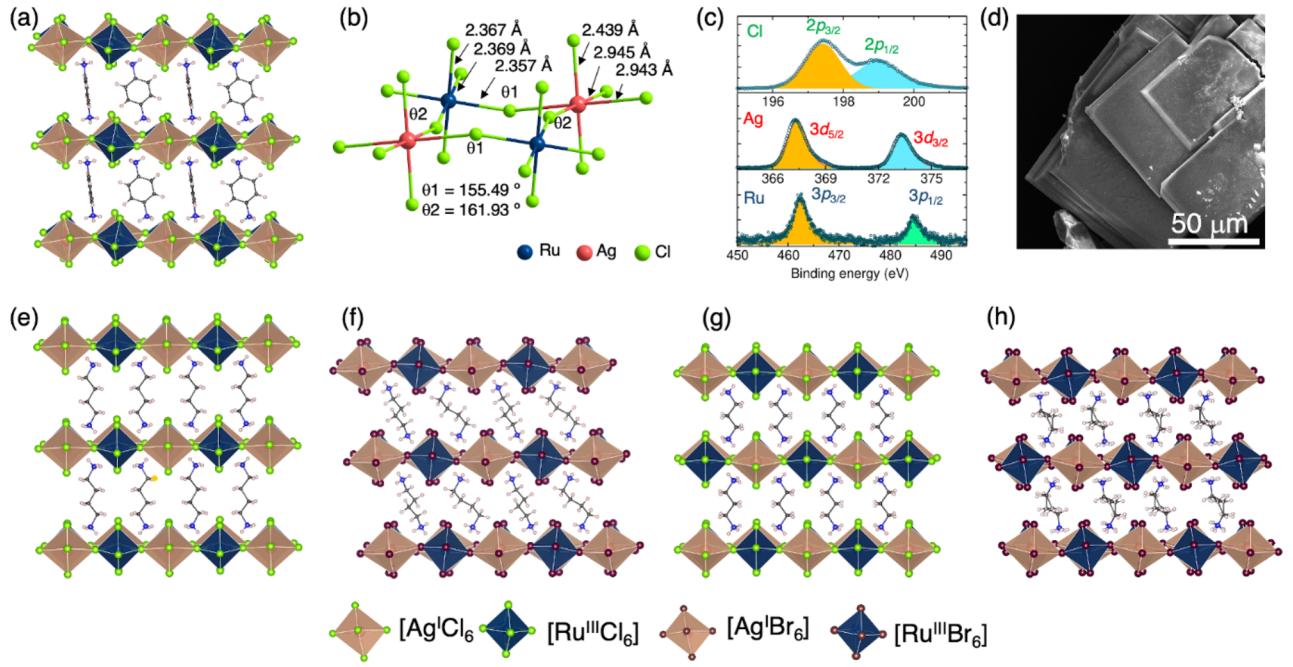

Figure 2. (a) Single-crystal X-ray structure of **1**. (b) Ball and stick model of **1** showing the bond lengths and in-plane connectivity of $[AgCl_6]$ and $[RuCl_6]$ octahedra. The $M^I{-}X{-}M^{III}$ bond angles are also given. (c) Core level Ru (3p), Ag (3d), and Cl (2p) XPS spectra of **1**. (d) SEM image of **1**. (e–h) Single-crystal X-ray structures of (e) **5**, (f) **6**, (g) **7**, and (h) **8**.

field stabilization energy (CFSE) associated with low-spin M^{III} ions.

Figures 2a and b show the crystal structure of **1** as a representative example of the $(PPDA)_2M^IM^{III}X_8$ series (**1** – **4**).

https://doi.org/10.1021/jacs.1c12760
J. Am. Chem. Soc. 2022, 144, 6661–6666

It has alternating [$AgCl_6$] and [$RuCl_6$] polyhedra in the perovskite layer and PPDA between the layers. The [$AgCl_6$] polyhedra exhibit shorter Ag−Cl_{ax} bonds (2.439 Å) than the Ag−Cl_{eq} bonds (2.943 and 2.945 Å) (Table S3). The [$RuCl_6$] octahedra exhibit Ru−Cl bond lengths of 2.357 Å, 2.367 Å, and 2.369 Å, of which the shortest and longest bonds are at the equatorial positions. Its elemental composition as well as the Ag^{I} and Ru^{III} oxidation states have been further confirmed by X-ray photoelectron spectroscopy (XPS) (Figure 2c, Figures S1−S3). The signs of higher oxidation states of Cu and Mo in the XPS spectra of **2** and **4** are likely due to surface oxidation. The SEM image of **1** shows a layer-by-layer morphology and crystal sizes in the micron range (Figure 2d). In the Cu^{I} analogue, **2**, the [$CuCl_6$] polyhedral are more distorted with much shorter Cu−Cl_{ax} bonds than the Ag−Cl_{ax} in **1**, while the equatorial bonds are comparable with those of **1**. Compound **2** is a rare example of a stable and fully ordered Cu^{I} based layered double perovskite chloride. The ordered Cu^{I}−In^{III} compounds, (BA or PEA)$_4$CuInCl$_8$ (BA = butylammonium;[22] PEA = phenethylammonium[23]), have been reported recently.

In the case of **3**, the in-plane separation between Ag and Ru metals increases due to the larger size of Br compared with Cl, while the interlayer gap changes marginally because of the comparable Ag−Br_{ax} and Ag−Cl_{ax} bond lengths. Although the Mo−Cl_{eq} lengths in **4** are longer than the corresponding Ru−Cl lengths in **1** and **2**, the in-plane Ag to Mo separation is comparable due to an increase in the in-plane octahedral tilting. Between the $M^{I}M^{III}X_8$ layers of compounds **1**−**4**, PPDA forms a herringbone pattern through C−H···π interactions; these are weaker in the bromide analogue. The $-NH_3^+$ groups exhibit N(H)···X hydrogen bonding interactions with the equatorial and axial halides, some of which are quite strong (<3.50 Å) (Table S4).[24] The shortest N···Cl distance of 3.0 Å is found in **4**, due to which the Ag^{I}−Cl−Mo^{III} angle is more twisted than in the other analogues (Figures S5−S9).

Figure 2e−h shows the structures of the Ag−Ru HLDP chlorides and bromides, **5**−**8**. These compounds show smaller twisting within the layers compared to the PPDA analogues (Figures S10−13), likely due to the flexibility of 1,4-BDA and 1,3-PDA. The 1,4-BDA spacer adopts an *anti* conformation in **5** (Figure S14). This conformation is typically found in layered perovskites at higher temperatures,[25,26] while the *gauche* conformation often forms at room temperature.[4,27−29] Notably, in the bromide compound **6**, 1,4-BDA exhibits two crystallographically unique cations in the *gauche* conformation. The 1,3-PDA spacer is present in the *anti* conformation, in the chloride **7**, while a mixed *anti* and *eclipsed* conformation (Figure S14) is found in the bromide analogue **8**. Interestingly, **7** shows a phase transition accompanied by a conformational change to mixed *anti* and *eclipsed* form of 1,3-PDA on cooling to 220 K (Figure S15). The 220 K phase shows no changes in either the space group or the layer stacking pattern, but the interlayer separation decreases from 9.11 to 8.64 Å and the structure resembles the bromide analogue **8**. In the 220 K phase, the [$AgCl_6$] and [$RuCl_6$] octahedra are axially compressed and equatorially expanded compared to the 300 K phase and these changes are more significant for [$AgCl_6$]. It seems that the stacking pattern in **1**−**8** is dependent on the alkyl chain length—the 4C chains of PPDA and 1,4-BDA form [0, 0] phases, while the 3C chain 1,3-PDA forms [1/2, 0] phases (Figure 1, see above); this is consistent with most previous reports on related compounds (Table S1). We have adopted a Glazer-like notation to describe the octahedral tilt systems in these compounds (Table 1).[30]

The band gaps of **1**−**4** lie in the range 1.55−2.05 eV (Figure 3a), which is comparable to some of the Bi^{III} HLDP iodides.[7]

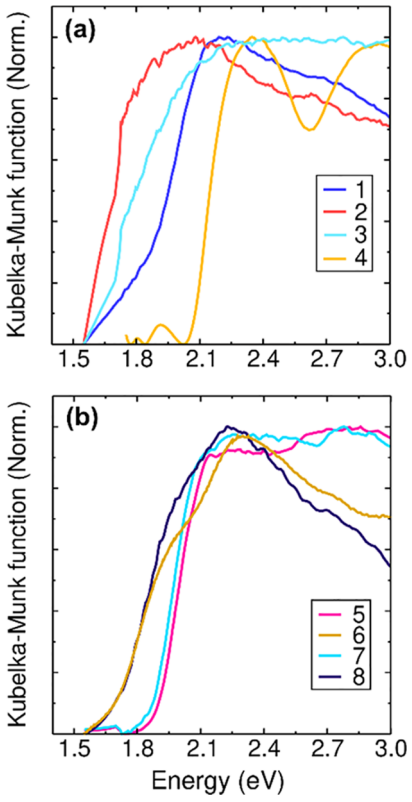

Figure 3. UV−visible absorption of HLDP halides. (a) Spectra of **1**−**4**; (b) Spectra of **5**−**8**.

Compound **1** shows a wider band gap than **2** and **3**, but it is narrower than **4**. The narrow band gap of **2** compared to **1** is consistent with $Cu^{I}Bi^{III}$ and $Ag^{I}Bi^{III}$ HLDP iodides reported elsewhere.[7] Because of the lower electronegativity of Br than Cl, the band gap of **3** is smaller than that of **1**. In addition to size and electronegativity, the M^{I}−X−M^{III} angles also influence the band gap. Specifically, deviations of the M^{I}−X−M^{III} angles from 180° lead to a decrease in the M−X orbital overlap, thereby increasing the band gap.[31] Compounds **5**−**8** with flexible spacers show band gaps comparable to those of the analogous PPDA perovskites (Figure 3b), suggesting that the organic spacers barely influence the electronic transitions. Earlier reports suggest that Pb-based hybrid layered perovskite iodides[32−34] and bromides[35,36] show slight band gap increase with increasing spacer length. We also note that the d−d transitions can be seen at 1.91, 2.31, and 2.90 eV in **4**, in agreement with previous work on K_3MoCl_6.[37] We did not observe any photoluminescent behavior. In future work, we shall be performing electronic structure calculations on this new family of compounds.

The magnetic susceptibilities of the compounds $(PPDA)_2Ag^{I}Ru^{III}Cl_8$ (**1**) and $(PPDA)_2Ag^{I}Mo^{III}Cl_8$ (**4**) were measured between 2 and 300 K, as described in the Supporting Information. These compounds feature widely separated Ru^{3+} and Mo^{3+} ions, of >7.18 Å and >7.31 Å, respectively, within the perovskite layers and are not expected to exhibit strong magnetic interactions. Note that the M^{III} to M^{III} distances between the layers are >10 Å (Table 1). Taking the results for **4** first, the data show excellent agreement with the Curie−Weiss law (Figure 4a). The derived magnetic moment, $\mu_{eff} = 3.78\ \mu_\beta$, is in very good

https://doi.org/10.1021/jacs.1c12760
J. Am. Chem. Soc. 2022, 144, 6661−6666

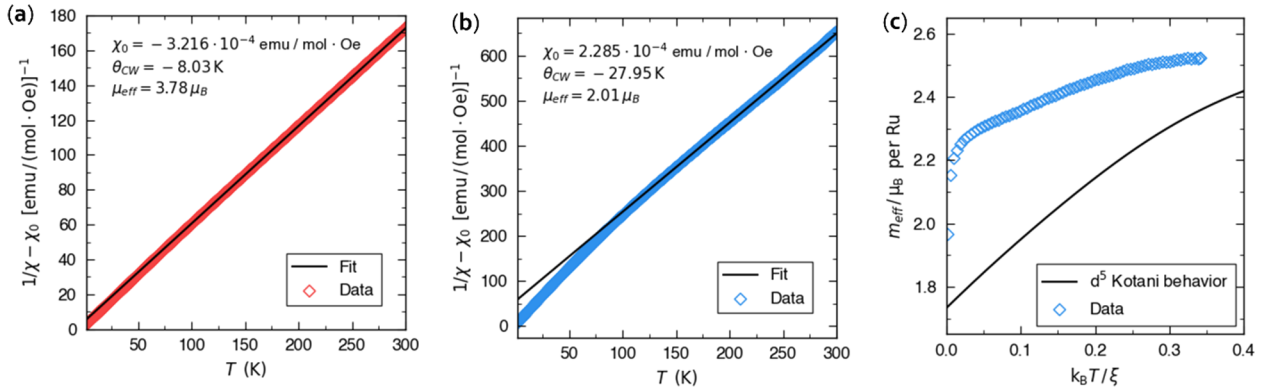

Figure 4. Magnetic data for the compounds $(PPDA)_2Ag^IMo^{III}Cl_8$ (**4**) and $(PPDA)_2Ag^IRu^{III}Cl_8$ (**1**). (a) Curie–Weiss fit for **4**; (b) Curie–Weiss fit for **1**; (c) Fitting of the magnetic moment data for **1** to the Kotani model with a spin–orbit coupling constant of 610 cm^{-1}.

agreement with the expected value of 3.87 μ_β for a spin-only t_{2g}^3 Mo^{3+} ion. The value of the Curie–Weiss theta, $\theta_{CW} = -8.03$ K, is indicative of weak antiferromagnetic coupling between the Mo^{III} ions. This is consistent with the long superexchange pathway that passes via the d^{10} Ag^I ion, i.e. Mo–Cl–Ag–Cl–Mo. Compound **4** is a rare example of an extended magnetic solid based upon a Mo^{III} halide. The molecular compound, K_3MoCl_6 (μ_{eff} = 3.83 μ_β; θ_{CW} = −5 K),[38] appears to be the closest magnetic analog of compound **4**. We also note that while α-$MoCl_3$ forms a 2D honeycomb lattice, it is diamagnetic at and below room temperature due to the formation of Mo–Mo bonds with a distance of 2.76 Å.[39] The magnetic behavior of $(PPDA)_2Ag^IRu^{III}Cl_8$ (**1**) is more complex due to the unquenched orbital angular momentum of the low spin t_{2g}^5 Ru^{III} ion. Fitting the high temperature data (150–300 K) to the Curie–Weiss law (Figure 4b) yields a moment, μ_{eff} of 2.01 μ_β and a θ_{CW} of −27.95 K. The larger θ_{CW} points to slightly stronger exchange coupling in **1** compared with **4**. If the variation of the magnetic moment with temperature is compared with the trend predicted by the Kotani theory for t_{2g}^5,[40] the fit is rather poor, irrespective of the choice of spin–orbit coupling constant (Figure 4c). The breakdown of the Kotani model for t_{2g}^5 is similar to our recent findings for other Ru^{III} compounds, e.g. $(CH_3NH_3)_2NaRuCl_6$.[25] There are several possible reasons for this, including deviations from perfect octahedral symmetry for Ru^{III} and breakdown of the assumption that the Ru^{III} ions are noninteracting. However, the geometry of the $RuCl_6$ unit in **1** is almost perfectly octahedral and the Ru···Ru distances are long (Table S3). Thus, we do not believe that the discrepancy can be explained on the basis of these two factors and it seems more likely that there is a need to revisit the Kotani theory for low-spin d^5 ions.

In conclusion, we have isolated and structurally characterized seven new hybrid layered perovskite halides of Ru^{III} and one of Mo^{III}. The results showcase that all the chemical components—including the organic diamine spacer, the monovalent metal, the trivalent metal, and the halide—are tunable, thereby significantly expanding the compositional and structural diversity of the HLDP halides family. We hope that these findings will serve as guidance for future developments in TM-based double perovskites, in terms of both new materials discoveries and applications.

■ ASSOCIATED CONTENT

Supporting Information

The Supporting Information is available free of charge at https://pubs.acs.org/doi/10.1021/jacs.1c12760.

Synthesis and characterization, scXRD refinement details, key bond lengths and bond angles, hydrogen bond interactions, powder X-ray diffraction patterns, X-ray photoelectron spectra (XPS), scanning electron microscope (SEM) images, additional single-crystal X-ray structures, octahedral tilting (PDF)

Accession Codes

CCDC 2122532–2122540 contain the supplementary crystallographic data for this paper. These data can be obtained free of charge via www.ccdc.cam.ac.uk/data_request/cif, or by emailing data_request@ccdc.cam.ac.uk, or by contacting The Cambridge Crystallographic Data Centre, 12 Union Road, Cambridge CB2 1EZ, UK; fax: + 44 1223 336033.

■ AUTHOR INFORMATION

Corresponding Authors

Ram Seshadri − *Materials Department and Materials Research Laboratory, University of California, Santa Barbara, California 93106, United States;* orcid.org/0000-0001-5858-4027; Email: seshadri@mrl.ucsb.edu

Anthony K. Cheetham − *Materials Department and Materials Research Laboratory, University of California, Santa Barbara, California 93106, United States; Department of Materials Science & Engineering, National University of Singapore, 117576 Singapore, Singapore;* orcid.org/0000-0003-1518-4845; Email: akc30@cam.ac.uk

Authors

Pratap Vishnoi − *Materials Department and Materials Research Laboratory, University of California, Santa Barbara, California 93106, United States; New Chemistry Unit and International Centre for Materials Science, Jawaharlal Nehru Centre for Advanced Scientific Research (JNCASR), Bangalore 560064, India;* orcid.org/0000-0003-4717-9346

Julia L. Zuo − *Materials Department and Materials Research Laboratory, University of California, Santa Barbara, California 93106, United States*

Xiaotong Li − *Department of Chemistry, Northwestern University, Evanston, Illinois 60208, United States;* orcid.org/0000-0001-7107-7273

Devesh Chandra Binwal − *New Chemistry Unit and International Centre for Materials Science, Jawaharlal Nehru Centre for Advanced Scientific Research (JNCASR), Bangalore 560064, India;* orcid.org/0000-0002-5418-8577
Kira E. Wyckoff − *Materials Department and Materials Research Laboratory, University of California, Santa Barbara, California 93106, United States;* orcid.org/0000-0003-4353-9447
Lingling Mao − *Materials Department and Materials Research Laboratory, University of California, Santa Barbara, California 93106, United States; Department of Chemistry, Southern University of Science and Technology (SUSTech), Shenzhen 518055, China;* orcid.org/0000-0003-3166-8559
Linus Kautzsch − *Materials Department and Materials Research Laboratory, University of California, Santa Barbara, California 93106, United States;* orcid.org/0000-0003-1999-436X
Guang Wu − *Department of Chemistry and Biochemistry, University of California, Santa Barbara, California 93106, United States*
Stephen D. Wilson − *Materials Department and Materials Research Laboratory, University of California, Santa Barbara, California 93106, United States*
Mercouri G. Kanatzidis − *Department of Chemistry, Northwestern University, Evanston, Illinois 60208, United States;* orcid.org/0000-0003-2037-4168

Complete contact information is available at: https://pubs.acs.org/10.1021/jacs.1c12760

Notes

The authors declare no competing financial interest.

■ ACKNOWLEDGMENTS

This work was supported by the Department of Energy, Office of Science, Basic Energy Sciences, under Grant No. SC0012541. P.V. thanks the Department of Science & Technology (DST) of Govt. of India for the Overseas Postdoctoral Visiting Fellowship (Award No. JNC/AO/A.0610-1(3)/2018-03), the Science & Engineering Research Board (SERB) of the Govt. of India for the Ramanujan Fellowship (Award No. RJF/2020/000106), and the Jawaharlal Nehru Centre for Advanced Scientific Research (JNCASR) Bangalore for the financial support and the research infrastructure. We acknowledge the shared facility of the Materials Research Science and Engineering Center (MRSEC) at the UC Santa Barbara under the National Science Foundation (NSF) Grant Number DMR 1720256. J.L.Z. also acknowledges the support of the NSF Graduate Research Fellowship Program under Grant No. 1650114. A.K.C. thanks the Ras al Khaimah Centre for Advanced Materials for financial support.

■ REFERENCES

(1) Smith, I. C.; Hoke, E. T.; Solis-Ibarra, D.; McGehee, M. D.; Karunadasa, H. I. A Layered Hybrid Perovskite Solar-Cell Absorber with Enhanced Moisture Stability. *Angew. Chem., Int. Ed.* **2014**, *53*, 11232−11235.
(2) Cao, D. H.; Stoumpos, C. C.; Farha, O. K.; Hupp, J. T.; Kanatzidis, M. G. 2D Homologous Perovskites as Light-Absorbing Materials for Solar Cell Applications. *J. Am. Chem. Soc.* **2015**, *137*, 7843−7850.
(3) Evans, H. A.; Mao, L.; Seshadri, R.; Cheetham, A. K. Layered Double Perovskites. *Annu. Rev. Mater. Res.* **2021**, *51*, 351−380.
(4) Mao, L.; Teicher, S. M. L.; Stoumpos, C. C.; Kennard, R. M.; DeCrescent, R. A.; Wu, G.; Schuller, J. A.; Chabinyc, M. L.; Cheetham, A. K.; Seshadri, R. Chemical and Structural Diversity of Hybrid Layered Double Perovskite Halides. *J. Am. Chem. Soc.* **2019**, *141*, 19099−19109.
(5) Jana, M. K.; Janke, S. M.; Dirkes, D. J.; Dovletgeldi, S.; Liu, C.; Qin, X.; Gundogdu, K.; You, W.; Blum, V.; Mitzi, D. B. Direct-Bandgap 2D Silver−Bismuth Iodide Double Perovskite: The Structure-Directing Influence of an Oligothiophene Spacer Cation. *J. Am. Chem. Soc.* **2019**, *141*, 7955−7964.
(6) Lassoued, M. S.; Bi, L.-Y.; Wu, Z.; Zhou, G.; Zheng, Y.-Z. Piperidine-Induced Switching of the Direct Band Gaps of Ag(I)/Bi(III) Bimetallic Iodide Double Perovskites. *J. Mater. Chem. C* **2020**, *8*, 5349−5354.
(7) Bi, L.-Y.; Hu, Y.-Q.; Li, M.-Q.; Hu, T.-L.; Zhang, H.-L.; Yin, X.-T.; Que, W.-X.; Lassoued, M. S.; Zheng, Y.-Z. Two-Dimensional Lead-Free Iodide-Based Hybrid Double Perovskites: Crystal Growth, Thin-Film Preparation and Photocurrent Responses. *J. Mater. Chem. A* **2019**, *7*, 19662−19667.
(8) Bi, L.-Y.; Hu, T.-L.; Li, M.-Q.; Ling, B.-K.; Lassoued, M. S.; Hu, Y.-Q.; Wu, Z.; Zhou, G.; Zheng, Y.-Z. Template Effects in Cu(I)−Bi(III) Iodide Double Perovskites: A Study of Crystal Structure, Film Orientation, Band Gap and Photocurrent Response. *J. Mater. Chem. A* **2020**, *8*, 7288−7296.
(9) Fu, D.; Wu, S.; Liu, Y.; Yao, Y.; He, Y.; Zhang, X.-M. A Lead-Free Layered Dion−Jacobson Hybrid Double Perovskite Constructed by an Aromatic Diammonium Cation. *Inorg. Chem. Front.* **2021**, *8*, 3576−3580.
(10) Li, X.; Traoré, B.; Kepenekian, M.; Li, L.; Stoumpos, C. C.; Guo, P.; Even, J.; Katan, C.; Kanatzidis, M. G. Bismuth/Silver-Based Two-Dimensional Iodide Double and One-Dimensional Bi Perovskites: Interplay between Structural and Electronic Dimensions. *Chem. Mater.* **2021**, *33*, 6206−6216.
(11) Ruan, H.; Guo, Z.; Lin, J.; Liu, K.; Guo, L.; Chen, X.; Zhao, J.; Liu, Q.; Yuan, W. Structure and Optical Properties of Hybrid-Layered-Double Perovskites $(C_8H_{20}N_2)_2AgMBr_8$ (M = In, Sb, and Bi). *Inorg. Chem.* **2021**, *60*, 14629−14635.
(12) Han, C.; Bradford, A. J.; Slawin, A. M. Z.; Bode, B. E.; Fusco, E.; Lee, S. L.; Tang, C. C.; Lightfoot, P. Structural Features in Some Layered Hybrid Copper Chloride Perovskites: $ACuCl_4$ or A_2CuCl_4. *Inorg. Chem.* **2021**, *60*, 11014−11024.
(13) Gregson, A. K.; Day, P.; Leech, D. H.; Fair, M. J.; Gardner, W. E. Magnetic Susceptibility and Magnetization of the Ionic Ferromagnets Dipotassium, Dirubidium, and Dicaesium Tetrachlorochromate(II). *J. Chem. Soc. Dalt. Trans.* **1975**, 1306−1311.
(14) Nakayama, Y.; Nishihara, S.; Inoue, K.; Suzuki, T.; Kurmoo, M. Coupling of Magnetic and Elastic Domains in the Organic−Inorganic Layered Perovskite-Like $(C_6H_5C_2H_4NH_3)_2Fe^{II}Cl_4$ Crystal. *Angew. Chem., Int. Ed.* **2017**, *56*, 9367−9370.
(15) Polyakov, A. O.; Arkenbout, A. H.; Baas, J.; Blake, G. R.; Meetsma, A.; Caretta, A.; van Loosdrecht, P. H. M.; Palstra, T. T. M. Coexisting Ferromagnetic and Ferroelectric Order in a $CuCl_4$-Based Organic−Inorganic Hybrid. *Chem. Mater.* **2012**, *24*, 133−139.
(16) Jaffe, A.; Mack, S. A.; Lin, Y.; Mao, W. L.; Neaton, J. B.; Karunadasa, H. I. High Compression-Induced Conductivity in a Layered Cu−Br Perovskite. *Angew. Chem., Int. Ed.* **2020**, *59*, 4017−4022.
(17) Castro-Castro, L. M.; Guloy, A. M. Organic-Based Layered Perovskites of Mixed-Valent Gold(I)/Gold(III) Iodides. *Angew. Chem., Int. Ed.* **2003**, *42*, 2771−2774.
(18) Vishnoi, P.; Seshadri, R.; Cheetham, A. K. Why Are Double Perovskite Iodides so Rare? *J. Phys. Chem. C* **2021**, *125*, 11756−11764.
(19) Banerjee, A.; Bridges, C. A.; Yan, J.-Q.; Aczel, A. A.; Li, L.; Stone, M. B.; Granroth, G. E.; Lumsden, M. D.; Yiu, Y.; Knolle, J.; Bhattacharjee, S.; Kovrizhin, D. L.; Moessner, R.; Tennant, D. A.; Mandrus, D. G.; Nagler, S. E. Proximate Kitaev Quantum Spin Liquid Behaviour in a Honeycomb Magnet. *Nat. Mater.* **2016**, *15*, 733−740.
(20) Vishnoi, P.; Zuo, J. L.; Strom, T. A.; Wu, G.; Wilson, S. D.; Seshadri, R.; Cheetham, A. K. Structural Diversity and Magnetic

Properties of Hybrid Ruthenium Halide Perovskites and Related Compounds. *Angew. Chem., Int. Ed.* **2020**, *59*, 8974−8981.
(21) Vishnoi, P.; Zuo, J. L.; Cooley, J. A.; Kautzsch, L.; Gómez-Torres, A.; Murillo, J.; Fortier, S.; Wilson, S. D.; Seshadri, R.; Cheetham, A. K. Chemical Control of Spin-Orbit Coupling and Charge Transfer in Vacancy-Ordered Ruthenium(IV) Halide Perovskites. *Angew. Chem., Int. Ed.* **2021**, *60*, 5184−5188.
(22) Connor, B. A.; Smaha, R. W.; Li, J.; Gold-Parker, A.; Heyer, A. J.; Toney, M. F.; Lee, Y. S.; Karunadasa, H. I. Alloying a Single and a Double Perovskite: A $Cu^{+/2+}$ Mixed-Valence Layered Halide Perovskite with Strong Optical Absorption. *Chem. Sci.* **2021**, *12*, 8689−8697.
(23) Aubrey, M. L.; Saldivar Valdes, A.; Filip, M. R.; Connor, B. A.; Lindquist, K. P.; Neaton, J. B.; Karunadasa, H. I. Directed Assembly of Layered Perovskite Heterostructures as Single Crystals. *Nature* **2021**, *597*, 355−359.
(24) Steiner, T. Hydrogen-Bond Distances to Halide Ions in Organic and Organometallic Crystal Structures: Up-to-Date Database Study. *Acta Crystallogr. Sect. B* **1998**, *54*, 456−463.
(25) Courseille, C.; Chanh, N. B.; Maris, T.; Daoud, A.; Abid, Y.; Laguerre, M. Crystal Structure and Phase Transition in the Perovskite-Type Layer Molecular Composite $NH_3(CH_2)_4NH_3PbCl_4$. *Phys. status solidi* **1994**, *143*, 203−214.
(26) Maris, T.; Bravic, G.; Chanh, N. B.; Leger, J. M.; Bissey, J. C.; Villesuzanne, A.; Zouari, R.; Daoud, A. Structures and Thermal Behavior in the Series of Two-Dimensional Molecular Composites NH_3-$(CH_2)_4$-NH_3MCl_4 Related to the Nature of the Metal M. Part 1: Crystal Structures and Phase Transitions in the Case *M* = Cu and Pd. *J. Phys. Chem. Solids* **1996**, *57*, 1963−1975.
(27) Han, Y.; Li, Y.; Wang, Y.; Cao, G.; Yue, S.; Zhang, L.; Cui, B.-B.; Chen, Q. From Distortion to Disconnection: Linear Alkyl Diammonium Cations Tune Structure and Photoluminescence of Lead Bromide Perovskites. *Adv. Opt. Mater.* **2020**, *8*, 1902051.
(28) Amami, M.; Zouari, R.; Ben Salah, A.; Burzlaff, H. 1,4-Butanediammonium Tetrachloromercurate(II). *Acta Crystallogr. Sect. E* **2002**, *58*, m357−m359.
(29) Shen, Y.; Liu, Y.; Ye, H.; Zheng, Y.; Wei, Q.; Xia, Y.; Chen, Y.; Zhao, K.; Huang, W.; Liu, S. Centimeter-Sized Single Crystal of Two-Dimensional Halide Perovskites Incorporating Straight-Chain Symmetric Diammonium Ion for X-Ray Detection. *Angew. Chem., Int. Ed.* **2020**, *59*, 14896−14902.
(30) McNulty, J. A.; Lightfoot, P. Structural Chemistry of Layered Lead Halide Perovskites Containing Single Octahedral Layers. *IUCrJ.* **2021**, *8*, 485−513.
(31) Vasileiadou, E. S.; Hadar, I.; Kepenekian, M.; Even, J.; Tu, Q.; Malliakas, C. D.; Friedrich, D.; Spanopoulos, I.; Hoffman, J. M.; Dravid, V. P.; Kanatzidis, M. G. Shedding Light on the Stability and Structure−Property Relationships of Two-Dimensional Hybrid Lead Bromide Perovskites. *Chem. Mater.* **2021**, *33*, 5085−5107.
(32) Safdari, M.; Svensson, P. H.; Hoang, M. T.; Oh, I.; Kloo, L.; Gardner, J. M. Layered 2D Alkyldiammonium Lead Iodide Perovskites: Synthesis, Characterization, and Use in Solar Cells. *J. Mater. Chem. A* **2016**, *4*, 15638−15646.
(33) Phuyal, D.; Safdari, M.; Pazoki, M.; Liu, P.; Philippe, B.; Kvashnina, K. O.; Karis, O.; Butorin, S. M.; Rensmo, H.; Edvinsson, T.; Kloo, L.; Gardner, J. M. Electronic Structure of Two-Dimensional Lead(II) Iodide Perovskites: An Experimental and Theoretical Study. *Chem. Mater.* **2018**, *30*, 4959−4967.
(34) Ma, C.; Shen, D.; Ng, T.-W.; Lo, M.-F.; Lee, C.-S. 2D Perovskites with Short Interlayer Distance for High-Performance Solar Cell Application. *Adv. Mater.* **2018**, *30*, 1800710.
(35) Kitazawa, N.; Aono, M.; Watanabe, Y. Excitons in Organic−Inorganic Hybrid Compounds $(C_nH_{2n+1}NH_3)_2PbBr_4$ (n = 4, 5, 7 and 12). *Thin Solid Films* **2010**, *518*, 3199−3203.
(36) Deng, C.; Zhou, G.; Chen, D.; Zhao, J.; Wang, Y.; Liu, Q. Broadband Photoluminescence in 2D Organic−Inorganic Hybrid Perovskites: $(C_7H_{18}N_2)PbBr_4$ and $(C_9H_{22}N_2)PbBr_4$. *J. Phys. Chem. Lett.* **2020**, *11*, 2934−2940.
(37) Kamalov, R. V.; Volkovich, V. A.; Polovov, I. B.; Vasin, B. D. Stability of Complex Molybdenum(III) Ions in Molten Alkali Metal Chlorides. *Russ. Metall.* **2012**, *2012*, 114−118.
(38) Van Dalen, P. A.; Steenland, M. J. Susceptibility Study of the Magnetic State of K_3MoCl_6. *Physica* **1967**, *36*, 275−288.
(39) McGuire, M. A.; Yan, J.; Lampen-Kelley, P.; May, A. F.; Cooper, V. R.; Lindsay, L.; Puretzky, A.; Liang, L.; KC, S.; Cakmak, E.; Calder, S.; Sales, B. C. High-Temperature Magnetostructural Transition in van Der Waals-Layered α-$MoCl_3$. *Phys. Rev. Mater.* **2017**, *1*, 64001.
(40) Kotani, M. On the Magnetic Moment of Complex Ions. (I). *J. Phys. Soc. Jpn.* **1949**, *4*, 293−297.

https://doi.org/10.1021/jacs.1c12760
J. Am. Chem. Soc. 2022, 144, 6661−6666